

Headline Articles

Emission Spectra and Relaxation Mechanism of b State O_2 in Low Temperature Ar Solids

Kenji Takizawa and Seiichiro Koda*

Department of Chemical System Engineering, School of Engineering, The University of Tokyo, Hongo 7-3-1, Bunkyo-ku, Tokyo 113-8656

(Received April 4, 2002)

The b → X emission of electronically excited O_2 isolated in Ar solids was observed under the pulsed KrF excimer laser irradiation at 248 nm. The relaxation proceeds along the b → a → b interstate transition. The time evolution of each b → X (v', v'') band was fitted by multi-exponential curves. The nonradiative rate is limited at the b → a transition due to the energy gap, which is larger than that of the a → b transition. The relaxation rate constants of individual vibrational levels ($v \leq 8$) of the b state were determined. The vibrational quantum number and temperature dependence of the nonradiative rate constants could be explained based on a multiphonon relaxation theory.

Condensed phase reactions are different from gas phase reactions in the point that the former always experience the influence of the surrounding molecules. The relaxation rates and mechanisms of excited states of simple molecules in simple surrounding media are thus some of the most fundamental types of information required for understanding the reactions in condensed phase. The photophysical behavior of laser excited O_2 isolated in rare gas solids is a typical example.

The energy levels, potentials and relaxation mechanism of O_2 doped in rare gas and N_2 solids in the neighborhood of the dissociation limit and below it have been studied so far mainly by means of absorption and emission spectroscopy as was reviewed recently.[1] Several studies have focused on the vibrational relaxation of electronic ground state $X^3\Sigma_g^-$, on the emission spectra from the Herzberg states ($A^3\Sigma_u^+$, $A'^3\Delta_u$, $c^1\Sigma_u^-$) which lie more than 4.1 eV above the ground state, and on the spectra from the low-lying $a^1\Delta_g$ (0.98 eV) and $b^1\Sigma_g^+$ (1.63 eV) states.

In the vibrationally excited O_2 ($X^3\Sigma_g^-$, v) in rare gas solids, an extremely slow vibrational relaxation, for example with the lifetime of more than 100 s for $v = 5$ in Ar solids, was reported.[1,2] Salloum and Dubost[2] tried successfully to explain this slow relaxation process, applying the theory of multiphonon relaxation proposed by Nitzan et al.[3] and later by Egorov and Skinner.[4] Consequently, the relaxation of X state was claimed to be an intramolecular multiphonon relaxation with the localized phonons. The vibrational level spacing in the X state is as large as ca. 1500 cm^{-1} and a very large number of phonons are needed for dissipating the energy along the relaxation progress into the lattice of the rare gas solids. As the result, the ground state vibrational relaxation is a very slow process.

The emission spectra from the Herzberg states (A, A′, c) have been measured by many researchers.[5–10] However, the spectra are mostly limited to those from the vibrationally relaxed levels. The vibrational relaxation in these excited electronic states is considered to be very fast. Numerous vibronic levels from the six electronic states (A, A′, c, b, a, X) exist in a relatively narrow energy range below the dissociation limit and the vibronic transitions may progress near-resonantly by adopting these levels. Such interstate relaxation processes are reviewed by Bondybey et al.[11]

The emission spectra from the vibrationally unrelaxed a and b states have been observed by several researchers,[12–16] though not in an extensive manner. In these states, which are different from the Herzberg states, only the three states (X, a and b) can interact due to energetic considerations, and the energy gaps between individual vibronic levels are relatively large. Therefore analysis of the time evolution of the emission spectra from these states should provide us information on the relaxation of the individual vibronic levels. However, only a very few reports have been published concerning the time evolution of vibrationally highly excited a and/or b states. Only one article described the lifetime of vibrationally excited b state with the measurement of the b → X(v', v'') emission spectra using the dissociative light irradiation.[16] However, the time evolutions of the vibrationally excited levels of the b state were not clearly obtained.

The objective of the present work is the quantitative measurement of relaxation rates among the a and b vibronic states in order to understand whether the mechanism of multiphonon relaxation is still valid in these vibronic levels of the electronically excited a and b state of O_2.

We studied as follows. At first, the A′ state was prepared by using a 248 nm pulsed laser to supply irradiation to the O_2 molecules isolated in Ar solids; then we observed the b → X(v', v'') emission spectra. From the time evolution of the individual vibronic transition bands, the production and decay process of the vibrational levels of the b state was kinetically analyzed so as to obtain their rise and decay rates.

Experimental

The experimental apparatus and sample preparation method were the same as described previously.[17] Briefly, a free-standing Ar solid of cubic structure, which was composed of micro-crystals, of ca. $10 \times 10 \times 10$ mm^3 size containing a small amount of O_2 (O_2/Ar = 1/50–1/10000), was prepared by the method of Schwentner et al.[18] The solid was typically kept at 16 K by a closed-cycle refrigerator in a vacuum chamber. The nominal purity of Ar and of O_2 gas obtained commercially were 99.9999% and 99.9995%, respectively.

The solid was irradiated by a KrF excimer laser at 248 nm (typical irradiation condition: laser fluence, 40 mJ pulse^{-1} cm^{-2}, irradiation area, 0.5 cm^2, repetition rate, 1 or 3 Hz) through a quartz window of the vacuum chamber. The resultant $b^1\Sigma_g^+ \rightarrow X^3\Sigma_g^-$ emission spectra were gathered with a lens at the perpendicular direction to the laser light, dispersed by a monochromator (HAMAMATSU, C5095; blaze wavelength, 600 nm) and detected by an ICCD detector (HAMAMATSU, PMA-100). The instrumental band-path width (FWHM) was 5 cm^{-1}. The wavelength was calibrated using an appropriate standard neon lamp within a precision of 2 cm^{-1} in the 650–850 nm region. In the time evolution measurement at a specific wavelength, the emission was dispersed by another monochromator (Nikon P-250; blazed wavelength of the grating, 750 nm; FWHM, 3 nm), detected by a photomultiplier (HAMAMATSU, R5509) and averaged by an oscilloscope (Le Croy, LS140). The time response for the time domain measurements was shorter than 1 μs.

Results

A. $b^1\Sigma_g^+ \rightarrow X^3\Sigma_g^-$ Emission Spectra. Under the KrF excimer laser irradiation to the O_2/Ar solid, a very intense banded emission identified with the $A'^3\Delta_u \rightarrow X^3\Sigma_g^-$ transition was observed in agreement with reports.[5,9,10] In parallel, another weaker banded emission was observed in the longer wavelength region; this was identified with the $b^1\Sigma_g^+ \rightarrow X^3\Sigma_g^-$ (v', v'') transition from the comparison with the literature.[16] The observed spectra using time gates after the laser pulse are shown in Fig. 1(a)–(e). The b → X (v', v'') emission spectra are shown in Fig. 1(b)–(e) and the corresponding transition energies are tabulated in Table 1. The spectroscopic constants for the b and X states have been obtained from the data in Table 1 and are compared with literature values[5,16] in Table 2.

B. Time Evolution of the b → X Emission. We observed the time evolution of each (v', v'') band for $v' - v'' = 0$–3, and confirmed that the bands from the same initial v' had identical time evolutions independent of v''. Thus we will show the time evolutions of the (v', $v'' = v'$) emission bands.

The time evolution of the individual b(v') → X(v'') emission intensity measurement at 16 K is shown by dots in Fig. 2. The maximum of each band intensity is normalized to unity. The initial component of the time evolution, which has a lifetime of ca. 100 μs at every (v', v'') band, is considered to be a contamination by the wing part of the strong A′ → X emission bands. The solid curves are fitting lines, as will be described later.

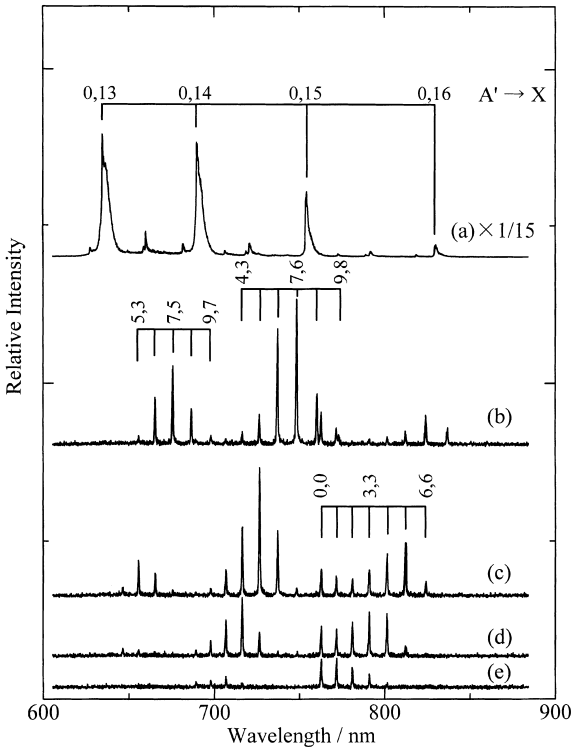

Fig. 1. b → X emission spectra at 16 K in O_2/Ar (1/1000) solid. The gate time is (a) from 0 to 0.5 ms, (b) from 5.0 to 5.5 ms, (c) from 20.0 to 20.5 ms, (d) from 50.0 to 50.5 ms, and (e) from 120.0 to 120.5 ms after the KrF laser pulsed irradiation. Some of the (v', v'') assignments are shown in the figure.

The (0, 0) band does not disappear within 1 s, the repetition period of the laser pulse, and thus the band intensity contains the contribution of the subsequent laser pulses. The bands other than the (0, 0) band disappear completely within 1 s. Apparently, the time evolution for each individual band has its specific rise and decay rate. A complex but still reproducible time evolution is observed for the (3, 3) band.

The time evolution of the b → X(v', v'') band measured at 30 K is also shown in Fig. 3. The comparison with the measurements at 16 K shows that the time evolution is apparently accelerated at the higher temperature with little change in the relative profiles.

C. Concentration Dependence of the b → X Emission. In order to check whether the guest O_2 molecule is isolated among the Ar host molecules, the concentration dependence of the b → X (v', v'') emission was examined by preparing solids with the concentration, [O_2]/[Ar], of 1/50, 1/100, 1/500, 1/1000 and 1/10000. In these solids, no prominent changes in relative intensity among the vibronic bands were found in spite of the concentration change. On the other hand, the time evolution of the band intensity showed clear concentration dependence. For instance, the time evolution of the b → X (4, 4) band is shown for different concentrations in Fig. 4. From the concentration of 1/50 to 1/500, both the "rise" and the "decay"

Table 1. Observed b → X Transition Energies in cm^{-1} in Ar Solid at 16 K

v'/v''	0	1	2	3	4	5	6	7	8	9	10
0	13106										
1	14504	12954									
2		14325	12798								
3			14143	12637							
4			15464	13955	12472						
5				15250	13762	12305					
6					15023	13562	12129				
7						14795	13355	11948			
8							14559	13149	11756		
9							15738	14320	12929		
10								15469	14073	12703	
11									15189	13816	12471
12										14907	13555

Table 2. Spectroscopic Constants in cm^{-1} for X and b States of O_2 in Ar Solid

	This work	Ref. 16	Ref. 5
$X^3\Sigma_g^-$			
ω_e	1586 ± 1	1581.07 ± 1.10	1569.5
$\omega_e x_e$	11.7 ± 0.1	12.70 ± 0.34	11.16
$\omega_e y_e$	—	0.07 ± 0.03	$\approx 10^{-4}$
$b^1\Sigma_g^+$			
T_e	13167 ± 3	13179.5 ± 1.1	
ω_e	1437 ± 1	1432.03 ± 1.13	
$\omega_e x_e$	14.6 ± 0.1	14.18 ± 0.283	
$\omega_e y_e$	—	−0.01 ± 0.02	

parts of the time evolution become slower with the decrease of the concentration. However, a further dilution from 1/500 to 1/10000 results in no apparent change anymore. The same tendency was observed for all v' levels.

Becker et al.[16] observed a $O_2 \cdot O_2$ dimol emission at 633 nm in O_2/Ar matrices by the energy pooling from two $O_2(a^1\Delta_g)$ molecules. They measured the b → X(0, 0), (1, 1) bands and found that the lifetime was independent of the O_2 concentration provided that the concentration was smaller than 1/100. Böhling et al.[14] reported that the $O_2 \cdot O_2$ dimol interaction was not observed at 1/400 concentration of O_2, in the b → X and a → X emission measurement in I_2/O_2/Ar matrices. It was also reported by Gudipati et al.[10] that the concentration dependence of the A′ → X emission intensity in O_2/Ar matrices changed linearly between the concentration of 1/500-1/1000, indicating no contribution of nonradiative process due to O_2–O_2 interactions.

From the present study described in Fig. 4 together with the above cited previous works, we conclude that the O_2 molecule can be regarded as isolated when the concentration is smaller than 1/500. In the following discussion, we employ the data obtained at the concentration of 1/1000.

Discussion

A. Generation Process of the b State. By the laser irradiation of 240–290 nm, O_2 in solid Ar is excited to Herzberg states ($A^3\Sigma_u^+$, $A'^3\Delta_u$, $c^1\Sigma_u^-$), mainly to the A′ state. O_2 in the A′ state emits the intense A′ → X emission. No emission from vibrationally excited O_2(A′) was observed; this is ascribed to the very fast vibrational relaxation (≤ 0.02 μs[8]) through the manifold of the A, A′ and c states. Besides the A′ (v = 0) → X radiative transition following the vibrational relaxation in the A, A′, c manifolds, some vibronic levels of the A, A′, c manifolds are considered to be transferred radiatively and/or nonradiatively to the b (v, v = 0–12) state whose generation was ev-

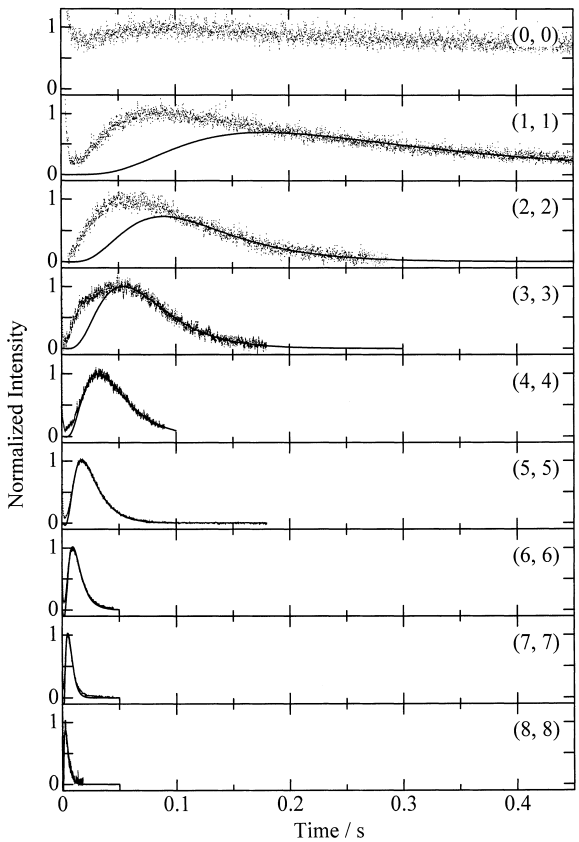

Fig. 2. Time evolution of the individual b → X (v', v'') emission intensity at 16 K. The dotted plots indicate the normalized emission intensities. The solid lines are fitting curves based on the interstate relaxation model represented by Eq. 11. In the $v \leq 3$ levels, the agreement between the experimental behavior and the fitting curve is not satisfactory and the experimental data for $v \leq 3$ are not used for the determination of the rate parameter.

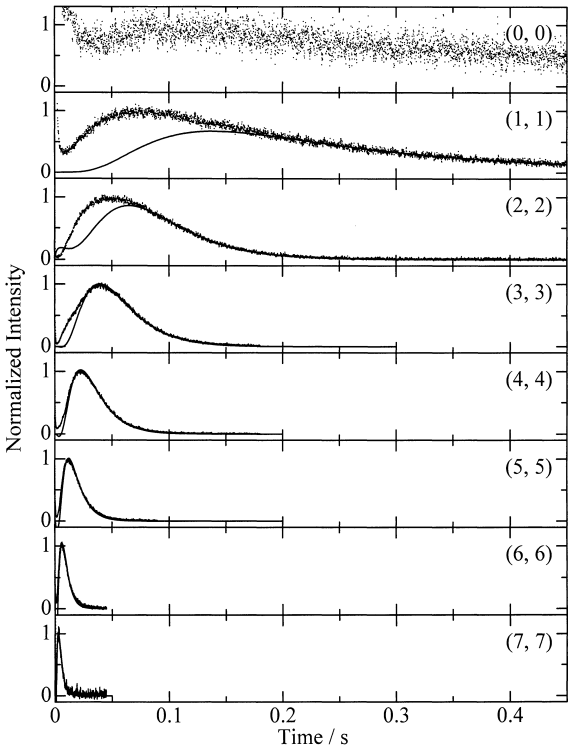

Fig. 3. Time evolution of the individual b → X (v', v'') emission intensity at 30 K. The dotted plots indicate the normalized emission intensities. The solid lines are fitting curves based on the interstate relaxation model represented by Eq. 11. In the $v \leq 3$ levels, the agreement between the experimental behavior and the fitting curve is not satisfactory and the experimental data for $v \leq 3$ are not used for the determination of the rate parameter.

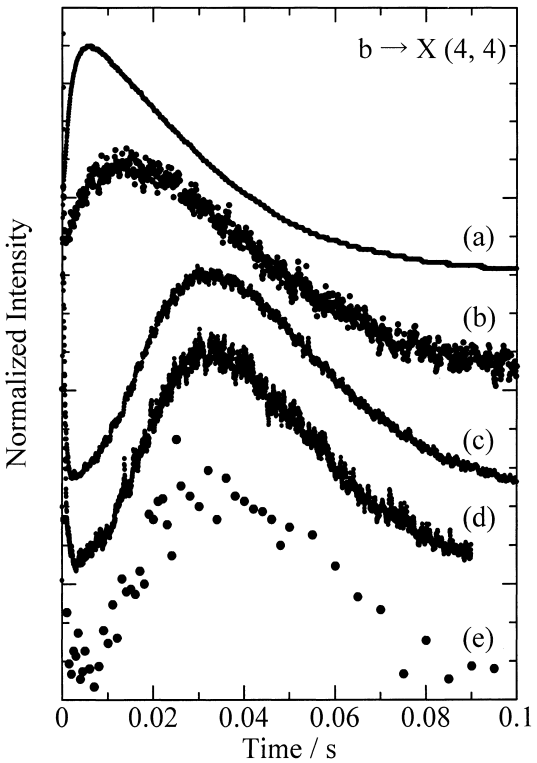

Fig. 4. Time evolution of the b → X (4, 4) emission intensity at 16 K for different O_2 concentrations. $[O_2]/[Ar]$ = (a) 1/50, (b) 1/100, (c) 1/500, (d) 1/1000, and (e) 1/10000.

idenced by the present emission spectra.

Firstly, we examine whether the b state is generated through direct radiative transition from the A, A′, c manifold. Experimentally, no emissions were observed except the A′ ($v = 0$) → X and b (at least up to $v' = 12$) → X emissions in 600–900 nm, which shows that no A, A′, c → b radiative transition occurs to any appreciable extent. If such transitions existed, they should have appeared in the same wavelength range. In addition, the b($v \leq 8$) state generation seems to necessitate a ms order time, as will be discussed later, which is much larger than the radiative lifetime of the A′ state of 80 μs.[5] Thus the radiative generation of the b state from the A, A′, c manifold is denied.

Secondly, we examine the possibility that the b state is generated through the nonradiative transition from the vibrationally excited X state. Let us consider, as one typical example, the transition from the X, $v = 18$ level to the most resonant b, $v = 8$ level through the following process,

$$^{16}O_2(X, v = 18) \rightarrow {}^{16}O_2(b, v = 8) + \Delta E, \Delta E \cong 1025\ cm^{-1}. \quad (1)$$

In this case the generation rate of the b, $v = 8$ level should be close to the decay rate of the X, $v = 18$ level. Eventually, the latter decay rate (1.7 s^{-1} in Ar matrix[2]) is much smaller than the former one ($\sim 10^3$ s^{-1}). Thus the A, A′, c manifolds → X → b process is excluded as the b state generation process.

Finally, two possible generation processes remain: one is the nonradiative A, A′, c manifolds → b transition and the other is the transition from the a state which is prepared by the nonradiative A, A′, c manifolds → a transition. We could not determine which is the principal generation process of the vibrationally excited b state. However, in either case, highly vibrationally excited b levels are generated and subsequently decay through the b and a vibronic levels as will be discussed in the following section.

B. Relaxation Process of Vibrationally Excited b State. When one considers the relaxation mechanism of the b state, the following information obtained by previous researchers should be taken into account.

Galaup et al.[13] observed the b, $v' \rightarrow$ a, $v''(v' \leq 3)$ emission bands which corresponded to $v' - v'' = 0, 1$ transitions. Tyczkowski et al.[15] also observed the b → a emission from the selectively excited b, $v' = 0$ level. The existence of nonradiative a, $v'' \rightarrow$ b, $v'(v'' - v' = 4)$ transition was also suggested. Becker et al.[16] reported the radiative decay rates of 40.8 ± 1.6 s^{-1} for the $v = 0$ and 1 levels of the b state in Ar matrix at 5 K. The b state intrastate relaxation rate for $v = 1 \rightarrow 0$ seems to be very small. They also measured the lifetime of 79 s for the a ($v = 0$) state. Thus the relaxation of the b state is expected to proceed through the b, $v' \rightarrow$ a, $v'' \rightarrow$ b, $v'-1 \rightarrow \cdots$ interstate nonradiative transition (b → a → b transition) accompanied by the b → a radiative transition.

C. Analysis of the Experimental Time Evolutions. According to the discussions in section B, we will quantitatively analyze the b → a → b transition. Though we detected

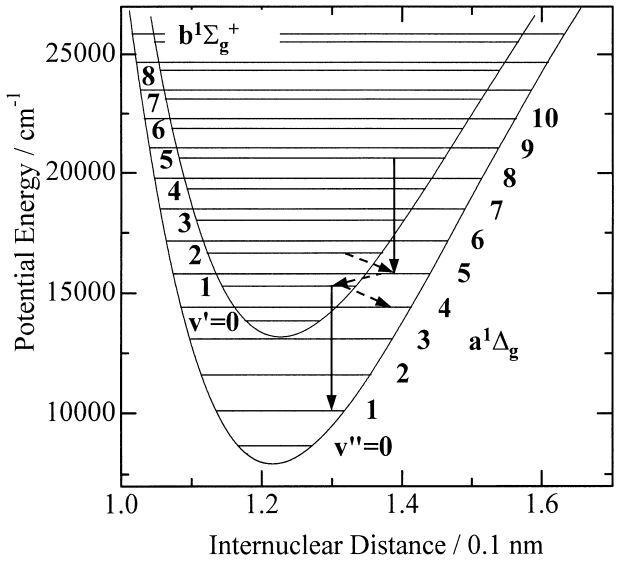

Fig. 5. Potential curves with the relevant vibronic energy levels of the b and a states of O_2 in Ar solids. The vertical arrows and the oblique arrows indicate the b → a emission and b → a → b interstate nonradiative transition, respectively, which are explained in Discussion C in the text.

the emission even from the $v = 12$ level of the b state, the time evolutions which allowed numerical analysis were limited to those for the levels lower than $v = 8$ due to the weakness of the higher bands.

For the analysis, we have at first determined the potential curves of the b and a states using the RKR method[19] with spectroscopic constants for the a and b state in Ar solids.[16] The potential curves together with the relevant vibronic energy levels in Ar solids are drawn in Fig. 5. Consulting the energy diagram in Fig. 5, we can illustrate the relevant relaxation process as follows.

$$O_2(b,v' = m + 4) \longrightarrow O_2(a,v'' = m + 4) + h\nu \quad (2a)$$

$$O_2(b,v' = m + 1) \xrightarrow{\text{nonradiative}} O_2(a,v'' = m + 4) \quad (2b)$$

$$O_2(a,v'' = m + 4) \xrightarrow{\text{nonradiative}} O_2(b,v' = m) \quad (3)$$

$$O_2(b,v' = m) \longrightarrow O_2(a,v'' = m) + h\nu \quad (4a)$$

$$O_2(b,v' = m) \xrightarrow{\text{nonradiative}} O_2(a,v'' = m + 3) \quad (4b)$$

In this scheme, "$m + i$" ($i = 1, 4$) represents the numerical value of the vibrational quantum number in the b and a states. Processes (2a) and (2b) are substantially identical with processes (4a) and (4b), respectively. The Franck–Condon maximum of individual b, $v' \rightarrow$ a, v'' radiative transitions is located at $v' = v''$. Therefore we mentioned only $v' = v''$ radiative transitions in the process (2a) and (4a) for simplicity. For the illustrative purpose, the relevant transitions for $m = 1$ are illustrated in Fig. 5. The energy gap between the a, v'' and b, v' levels is the smallest for $v'' - v' = 4$. Thus the m level of the b state is nonradiatively generated from $m + 4$ level of the a state as expressed by process (3), and decays through the b → a nonradiative transition by process (4b) together with the b → a radiative transition by process (4a).

The above-mentioned b → a → b relaxation process is described by the following equations:

$$\frac{dN^{a}_{v''=m+4}(t)}{dt} = \sum_{n \geq m+1} k^{b\rightarrow a,rad}_{v'=n,v''=m+4} S_{v'=n,v''=m+4} N^{b}_{v'=n}(t) + k^{b,nrad}_{v'=m+1} N^{b}_{v'=m+1}(t) - k^{a,nrad}_{v''=m+4} N^{a}_{v''=m+4}(t) \quad (5)$$

$$\frac{dN^{b}_{v'=m}(t)}{dt} = k^{a,nrad}_{v''=m+4} N^{a}_{v''=m+4}(t) - \left(k^{b,nrad}_{v'=m} + k^{b,rad}_{v'=m}\right) N^{b}_{v'=m}(t) \quad (6)$$

where $N^{b}_{v'=m}(t)$ and $N^{a}_{v''=m+4}(t)$, $k^{b,nrad}_{v'=m}$ and $k^{a,nrad}_{v''=m+4}$ are the populations and the nonradiative relaxation rate constants of the b, m and a, $m + 4$ levels, respectively. $S_{v'=n,v''=m+4}$ and $k^{b\rightarrow a,rad}_{v'=n,v''=m+4}$ are the Franck-Condon factor and the radiative rate constant of the b, $n \rightarrow$ a, $m + 4$ transition, respectively. $k^{b,rad}_{v'=m}$ is the radiative rate constant, and

$$k^{b,rad}_{v'=m} = \sum_{m'} k^{b\rightarrow a,rad}_{v'=m,v''=m'} = \text{const} \times \sum_{m'} \omega^{3}_{v'=m,v''=m'} S_{v'=m,v''=m'}, \quad (7)$$

where $\omega_{v'=m,v''=m'}$ is the b, $m \rightarrow$ a, m' transition energy. In the later numerical evaluation, $k^{b,rad}_{v'=0}$ at 16 and 30 K are evaluated from Fig. 3 in Ref. 16. And the initial population, , $N^{b}_{v'=m}(0)$ is set at zero.

To solve Eqs. 5 and 6, we will make the following simplifications:

(a) The energy of the a, $m + 4 \rightarrow$ b, m transition is by more than 280 cm^{-1} smaller than the preceding b, $m + 1 \rightarrow$ a, $m + 4$ transition. Therefore the former transition is much faster than the latter transition and then

$$\frac{dN^{a}_{v''=m+4}(t)}{dt} \approx 0 \quad (8)$$

is derived. Thus,

$$\sum_{n \geq m+1} k^{b\rightarrow a,rad}_{v'=n,v''=m+4} S_{v'=n,v''=m+4} N^{b}_{v'=n}(t) + k^{b,nrad}_{v'=m+1} N^{b}_{v'=m+1}(t) = k^{a,nrad}_{v''=m+4} N^{a}_{v''=m+4}(t) \quad (9)$$

(b) In the higher vibrational levels (eventually $v' \geq 4$, as will be discussed later), the first term of the left hand side of Eq. 9 is negligibly small compared to the other two terms, considering the relatively fast nonradiative character of the higher vibrational levels. Then,

$$k^{b,nrad}_{v'=m+1} N^{b}_{v'=m+1}(t) = k^{a,nrad}_{v''=m+4} N^{a}_{v''=m+4}(t) \quad (10)$$

In the lower vibrational levels where the nonradiative process becomes slow compared to the radiative process, this approximation is no longer valid, as will be discussed later.

Under the simplification (a) and (b), the time evolution of $N^{b}_{v=m}(t)$ is described by

$$\frac{dN^{b}_{v=m}(t)}{dt} = k^{b,nrad}_{v=m+1}N^{b}_{v=m+1}(t) - \left(k^{b,nrad}_{v=m} + k^{b,rad}_{v=m}\right)N^{b}_{v=m}(t). \quad (11)$$

Hereafter both of v' and v'' in the preceding nomenclature are replaced by v for the most part. Solving the series of equations as follows, we obtain the time evolution of the b, v ($v \leq 8$) populations. The emission intensity from the integrated form of Eq. 11 can be approximately described as

$$N^{b}_{v=m}(t) = \gamma I^{b}_{v=m}(t) = \alpha\left\{\exp\left(-k^{b}_{v=m}t\right) - \beta\exp\left(-k^{b}_{v=m+1}t\right)\right\} \quad (12)$$

where $I^{b}_{v=m}(t)$ is the b $\rightarrow$ X emission intensity from the b, m level and $k^{b}_{v=m} = k^{b,nrad}_{v=m} + k^{b,rad}_{v=m}$. γ is introduced in order to relate the population to the observed intensity. Because the detection sensitivity could not be kept common for all of the time evolution measurements, γ, and thus α also, is a parameter dependent on the m number. On the other hand, the parameter β is introduced so as to compensate the contributions from the higher vibrational levels ($m > 9$). If there is no population in the higher vibrational levels, β would be unity. If there is any contribution from the higher levels, β is not unity and will be determined so as to give the best fit between the prediction and the experimental time evolution. The detailed relationship between β and the contribution from the higher levels will be found in the Appendix.

At first, the experimental time evolution for $m = 8$ in Fig. 2 was fitted by Eq. 12 as explained above. We obtained $N^{b}_{v=8}(t)$ and thus determined $k^{b}_{v=8}$, $k^{b}_{v=9}$, and β, which were then applied to solve Eq. 11 for $m = 7$, where the fitting parameter was $k^{b}_{v=7}$. The procedure was successively repeated down to $m = 1$ level, and we determined the relaxation rate constants related to individual vibrational levels. The fitting curves for the individual time evolutions are also drawn in Figs. 2 and 3 by solid lines.

The k^{b}_{v} values determined through the fitting procedure for the experiments at 16 and 30 K are listed in Table 3 together with the individual radiative rate constants of the b, v level, $k^{b,rad}_{v}$. The latter values were calculated using Eq. 7, where the "const." value was determined so as to reproduce the value experimentally obtained by Becker et al.[16] at $v = 0$. The required Franck–Condon factors were evaluated using the RKR method.[19]

The determined k^{b}_{v} values explained both the rise and decay behaviors satisfactorily for $v \geq 4$ levels. However, in $v = 3 - 1$ levels, the fitting procedure could not reproduce the experimental behavior in the initial stage, where we found a much larger population in the experiments than in the fittings. Therefore we determined k^{b}_{v} values in $v = 3 - 1$ levels so as to reproduce only the slower part of each time evolution. The results are already shown in Figs. 2 and 3. The large initial population may be caused by the non-negligible contribution of the first radiative term in Eq. 5. Taking into account the first radiative term in Eq. 5, the time evolution of $N^{b}_{v=m}(t)$ can be written as

$$N^{b}_{v=m}(t) = e^{-k^{b}_{v=m}t}\int_{0}^{t}\left\{\sum_{n\geq m+1}k^{b\rightarrow a,rad}_{v'=n,v''=m+4}S_{v'=n,v''=m+4}N^{b}_{v'=n}(t) + k^{b,nrad}_{v'=m+1}N^{b}_{v'=m+1}(t)\right\}e^{k^{b}_{v=m}t}dt, \quad (13)$$

where we employ the functions of $N^{b}_{v'=n}(t)$ which are obtained from the fitting curves for higher vibrational levels.

After application of Eq. 13, the improved fitting curves satisfactorily reproduced the initial experimental behaviors in $v =$ 1–3 levels. As an example, the comparison of experimental data with the fitting curve in $v = 3$ is shown in Fig. 6. It is worthy to note that the k^{b}_{v} ($v =$ 1–3) values are not substantially affected by the inclusion of the first term of Eq. 5. Thus the initial time behavior of the lower v levels can be interpreted by taking into account the contribution of radiative process from the higher levels. However, the fitting may not be unique, and thus we kept the k^{b}_{v} values for the $v \leq 3$ levels undetermined.

D. Analysis of the Relaxation Rates on the Basis of a Multiphonon Relaxation Theory. The relaxation rate constant for each b, v level, k^{b}_{v}, was determined through the fitting procedure as described in the previous section. The nonradiative rate constant ($v \geq 4$) is then evaluated from the relation $k^{b,nrad}_{v} = k^{b}_{v} - k^{b,rad}_{v}$ and is plotted in Fig. 7.

The $k^{b,nrad}_{v}$ value increases almost exponentially with the in-

Table 3. Relaxation Rate Constants of the b, v Levels at 16 and 30 K and Relevant Franck–Condon Factors

		16 K				30 K			
v	$S_{v,v'}$	k^{b}_{v}/s^{-1}	r[a)]	$k^{b,rad}_{v}/s^{-1}$	$k^{b,nrad}_{v}/s^{-1}$	k^{b}_{v}/s^{-1}	r[a)]	$k^{b,rad}_{v}/s^{-1}$	$k^{b,nrad}_{v}/s^{-1}$
0	4.2×10^{-7}	—		44[b)]	—	—		50[b)]	—
1	2.0×10^{-6}	—		42	—	—		48	—
2	5.9×10^{-6}	—		40	—	—		46	—
3	1.4×10^{-5}	—		39	—	—		44	—
4	2.9×10^{-5}	48	0.99	37	11	68	0.99	43	25
5	5.6×10^{-5}	82	0.99	36	46	111	0.99	41	70
6	9.9×10^{-5}	150	0.99	35	115	249	0.99	40	209
7	1.7×10^{-4}	383	0.99	33	350	513	0.99	38	475
8	2.7×10^{-4}	520	0.98	32	488	543	0.99	37	506
9	4.3×10^{-4}	654	0.98	31	623	—		35	—

a) r is the correlation coefficient in the fitting procedure using Eq. 11.
b) The values of $k^{b,rad}_{0}$ are evaluated from Fig. 3 in Ref. 16.

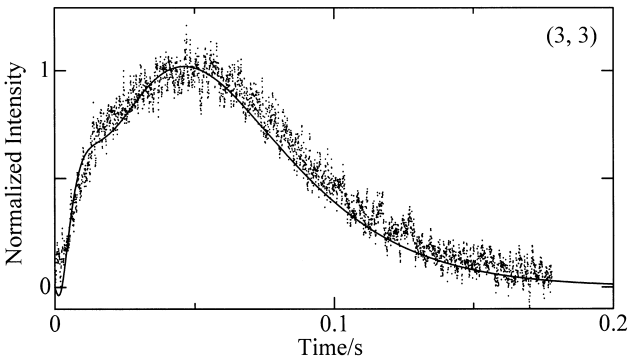

Fig. 6. Time evolution of the b → X (3, 3) emission intensity at 16 K. The plots indicate the normalized emission intensities. The solid line is improved fitting curve represented by Eq. 13.

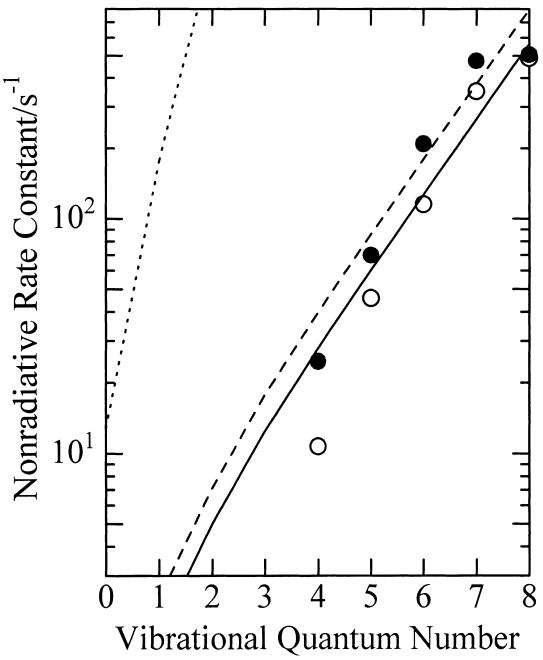

Fig. 7. The v dependence of the nonradiative relaxation rate constants for the b, v levels. The open circles and filled circles are experimental data at 16 and 30 K, respectively. The solid curves and dashed curves are the multiphonon relaxation rate at 16 and 30 K calculated by Eqs. 14 and 15 in the text. The dotted curve is the calculated a → b interstate relaxation rate at 16 K.

crease of the vibrational quantum number of the b state. In order to explain the vibrational quantum number and temperature dependence of the nonradiative rate constant, we will employ the theory of multiphonon relaxation. According to Bachir et al.,[20] the rate constant of interstate relaxation is equated as follows:

$$k_v^{\mathrm{nrad}}(0) \propto C_{\mathrm{el}} \frac{S_{v,v'}}{\eta!}, \tag{14}$$

$$\frac{k_v^{\mathrm{nrad}}(T)}{k_v^{\mathrm{nrad}}(0)} \cong (1 + \bar{n})^{\eta} \mathrm{e}^{2\bar{n}}. \tag{15}$$

Equations 14 and 15 indicate vibrational quantum number and temperature dependence of the relaxation rate constant, respectively. Here C_{el} is the electronic coupling element; η, the number of necessary phonons to supply the energy gap; v, the vibrational quantum number; T, the temperature (16 or 30 K); $\bar{n} = \{\exp(h\nu_{\mathrm{p}}/k_{\mathrm{B}}T) - 1\}^{-1}$, the phonon occupation number; and ν_{p}, the phonon frequency. $S_{v,v'}$ is the abridged charactor of $S_{v'=n,v''=m+4}$. Such values are tabulated in Table 3. $k_v^{\mathrm{nrad}}(0)$ is the nonradiative rate constant at $T = 0$. We calculated the nonradiative rate constants of individual v levels of the b state by employing Eqs. 13 and 14. Assuming that the phonon density of state is continuous against energy, we employed the Stirling's approximation for evaluating η:

$$\eta! = \eta^{\eta}\mathrm{e}^{-\eta}\sqrt{2\pi\eta}. \tag{16}$$

According to Salloum and Dubost[2], a localized phonon with a frequency of $\nu_{\mathrm{p}}/2\pi c = 75 \pm 5$ cm^{-1} in O_2-doped Ar matrix was adopted in the calculation, although the Debye frequency of solid Ar is $\nu_{\mathrm{p}}/2\pi c = 64$ cm^{-1}.[21] The calculated $k_v^{\mathrm{b,nrad}}$ values are shown in Fig. 7 with a solid curve at 16 K and with a dashed curve at 30 K. Since Eq. 14 is a proportionality equation, the curves were shifted so as to yield a best fit with the experiments. The vibrational quantum number dependence in the calculation based on the localized phonon mode agrees well with the experimental dependence.

If the C_{el} values for the a → b and b → a vibronic transitions do not differ appreciably from each other, both vibronic transition rates can be determined relatively by employing the individual Franck-Condon factors and energy gaps. Thus obtained rate constants of the a → b multiphonon transition at 16 K are also drawn in Fig. 7 with a dotted curve. The necessary numbers of the localized phonons for energy matching for the b, v → a, $v + 3$ and the a, $v + 4$ → b, v transitions are ca. 11 and 5–8 for $v \leq 8$ of the b state, respectively. Therefore, a → b nonradiative rate constants are more than 2 orders of magnitude larger than those of the b → a transition.

From Eq. 15, we estimated the ratio for $k_v^{\mathrm{b,nrad}}$ values at 30 K against those at 16 K to be $k_v^{\mathrm{b,nrad}}$ (30 K)/$k_v^{\mathrm{b,nrad}}$(16 K) = 1.4 ± 0.01 for the b → a transition in the range of v = 1–8 of the b state. The experimental value was found to be 1.6 ± 0.2 for the v = 4–8 levels, which is fair in agreement with the estimation.

Judging from the above vibrational quantum number and temperature dependence of the rate constant, we can confidently conclude that the dominant route of vibrational relaxation for the b state is the b → a → b interstate relaxation. For this relaxation route, the relaxation rate constants of individual steps could be explained satisfactorily by means of the multiphonon relaxation theory.

Assuming that the difference of the intrastate vibrational relaxation rate between the b and the X state was caused only by their different vibrational energy gaps, we estimated the intrastate relaxation rate constants of the b state in the same procedure as the vibrational multiphonon relaxation of the X state.[2] On this assumption the intrastate relaxation rate constants of

the b state were found to be more than 10^3 times smaller than those of the b → a → b interstate relaxation in b, $v \leq 8$ levels. This consideration further supports the interstate b → a → b relaxation process.

Conclusions

The vibrational relaxation of the b, v levels of O_2 isolated in Ar solids was pursued by observing the time evolution of the emission intensity of the corresponding b → X transition. The time evolution curves were analyzed to obtain relevant nonradiative rate constants that were interpreted by the multiphonon relaxation theory. The following conclusions were obtained.

1. The dominant relaxation route is the b → a → b interstate transition.

2. In the higher vibrational levels ($v \geq 4$) of the b state, the transition rate is mainly determined nonradiatively.

3. The initial rapid rise of the population in lower vibrational levels ($v \leq 3$) of the b state can be explained by taking into account the radiative transition from the higher vibrational levels of the b state to the a state.

4. The nonradiative transition rate is much smaller in the b → a transition than in the subsequent a → b transition due to the larger energy gap in the former transition.

5. The vibrational quantum number and temperature dependence of the b → a nonradiative rate constant is satisfactorily explained by the multiphonon relaxation theory employing the localized phonons.

Appendix

Analysis of the Time Evolution Using Eq. 12. In the solution of the rate Eq. 11, a parameter β was employed in the second term of Eq. 12. The meaning of β is the following:

We consider the relaxation in the b state,

$$\frac{dN^{b}_{v=m}(t)}{dt} = k^{b,nrad}_{v=m+1}N^{b}_{v=m+1}(t) - \left(k^{b,nrad}_{v=m} + k^{b,rad}_{v=m}\right)N^{b}_{v=m}(t). \tag{11}$$

In Eq. 11 the $m + 1$ level is generated and relaxed to the m level. If the population of the $m + 1$ level, $N^{b}_{v=m+1}(t)$, is expressed as,

$$N^{b}_{v=m+1}(t) = N^{b}_{v=m+1}(0)e^{-\left(k^{b,nrad}_{v=m+1} + k^{b,rad}_{v=m+1}\right)t}, \tag{A1}$$

then Eq. 11 can be integrated analytically by substitution of the above $N^{b}_{v=m+1}(t)$ into Eq. 11. The solution of $N^{b}_{v=m}(t)$is

$$N^{b}_{v=m}(t) = \frac{k^{b,nrad}_{v=m+1}}{k^{b,nrad}_{v=m+1} - k^{b,nrad}_{v=m}}N^{b}_{v=m+1}(0) \times \left(e^{-\left(k^{b,nrad}_{v=m} + k^{b,rad}_{v=m}\right)t} - e^{-\left(k^{b,nrad}_{v=m+1} + k^{b,rad}_{v=m+1}\right)t}\right). \tag{A2}$$

In the same way, we solve Eq. 11 successively and the population, $N^{b}_{v=m-1}(t)$, is obtained as shown below:

$$N^{b}_{v=m-1}(t) = \frac{k^{b,nrad}_{v=m-1}k^{b,nrad}_{v=m}}{(k^{b,nrad}_{v=m+1} - k^{b,nrad}_{v=m-1})(k^{b,nrad}_{v=m} - k^{b,nrad}_{v=m-1})}N^{b}_{v=m+1}(0) \times \left(e^{-\left(k^{b,nrad}_{v=m-1} + k^{b,rad}_{v=m-1}\right)t} - \frac{k^{b,nrad}_{v=m+1} - k^{b,nrad}_{v=m-1}}{k^{b,nrad}_{v=m+1} - k^{b,nrad}_{v=m}}e^{-\left(k^{b,nrad}_{v=m} + k^{b,rad}_{v=m}\right)t} + \frac{k^{b,nrad}_{v=m} - k^{b,nrad}_{v=m-1}}{k^{b,nrad}_{v=m+1} - k^{b,nrad}_{v=m}}e^{-\left(k^{b,nrad}_{v=m+1} + k^{b,rad}_{v=m+1}\right)t}\right). \tag{A3}$$

We will consider the case of $v = 8$. If the pulsed laser excitation generates the $v = 9$ level at the beginning, the population of the b, $v = 8$ level would be written by Eq. A2 and the value of β in Eq. 12 is unity. On the other hand, if the initial excited state is $v = 10$, 11 or a higher level, the population of the $v = 8$ level is written by Eq. A3 or by a more complicated multi-exponential equation. Instead of employing the multi-exponential equation faithfully as a fitting function, we describe the contribution from higher terms by introducing a parameter β as a coefficient of the second term. Namely,

$$-\frac{k^{b,nrad}_{v=m+1} - k^{b,nrad}_{v=m-1}}{k^{b,nrad}_{v=m+1} - k^{b,nrad}_{v=m}}e^{-\left(k^{b,nrad}_{v=m} + k^{b,rad}_{v=m}\right)t} + \frac{k^{b,nrad}_{v=m} - k^{b,nrad}_{v=m-1}}{k^{b,nrad}_{v=m+1} - k^{b,nrad}_{v=m}}e^{-\left(k^{b,nrad}_{v=m+1} + k^{b,rad}_{v=m+1}\right)t} \rightarrow \beta e^{-\left(k^{b,nrad}_{v=m} + k^{b,rad}_{v=m}\right)t}, \tag{A4}$$

Based on this approximation, we employ Eq. 12 as the fitting function of the $v = 8$ level of the b state. The agreement between the experimental time evolution for the b, $v = 8$ level and the fitting curve of Eq. 12 was satisfactory. Here the adopted β was 1.1, which shows that the contributions from the higher levels are negligibly small.

The present work is supported by a Grant-in-Aid for Scientific Research (A) from the Ministry of Education, Science and Culture of Japan (No. 12305051), which is greatly appreciated.

References

1 S. Koda and H. Kajihara, *Bull. Chem. Soc. Jpn.*, **70**, 1225 (1997).

2 A. Salloum and H. Dubost, *Chem. Phys.*, **189**, 179 (1994).

3 A. Nitzan, S. Mukamel, and J. Jortner, *J. Chem. Phys.*, **63**, 200 (1975).

4 S. A. Egorov and J. L. Skinner, *J. Chem. Phys.*, **106**, 1034 (1997).

5 J. Goodman and L. E. Brus, *J. Chem. Phys.*, **67**, 1482 (1977).

6 J. Goodman and L. E. Brus, *J. Chem. Phys.*, **67**, 4398 (1977).

7 J. Goodman and L. E. Brus, *J. Chem. Phys.*, **67**, 4408 (1977).

8 R. Rossetti and L. E. Brus, *J. Chem. Phys.*, **71**, 3963 (1979).

9 F. Okada, H. Kajihara, and S. Koda, *Chem. Phys. Lett.*, **192**, 357 (1992).

10 M. S. Gudipati, F. Schouren, M. Kalb, and R. Wagner, *Spectrochim. Acta Part A*, **56**, 2581 (2000).

11 V. E. Bondybey, M. Räsänen, and A. Lammers, *Annu. Rep. Prog. Chem., Sect. C*, **95**, 331 (1999).

12 H. Dubost, J. P. Galaup, and R. Charneau, *J. Luminescence*, **38**, 147 (1987).

13 J. P. Galaup, R. Charneau, and H. Dubost, *J. Luminescence*, **40&41**, 250 (1988).

14 R. Böhling, A. C. Becker, B. F. Minaev, K. Seranski, and U. Schurath, *Chem. Phys.*, **142**, 445 (1990).

15 G. Tyczkowski, U. Schurath, M. Bodenbinder, and H. Willner, *Chem. Phys.*, **215**, 379 (1997).

16 A. C. Becker, U. Schurath, H. Dubost, and J. P. Galaup, *Chem. Phys.*, **125**, 321 (1988).

17 H. Kajihara, T. Okamura, and S. Koda, *Chem. Phys. Lett.*, **256**, 126 (1996).
18 N. Schwentner, O. Doessel, and H. Nahme, *Laser Techniques for Extreme Ultraviolet Spectroscopy, AIP Conf. Proc.*, **90**, 163 (1982).
19 H. Telle and U. Telle, *Comput. Phys. Commun.*, **28**, 1 (1982).
20 I. H. Bachir, R. Charneau, and H. Dubost, *Chem. Phys.*, **164**, 451 (1992).
21 L. X. Finegold and N. E. Phillips, *Phys. Rev.*, **177**, 1383 (1969).